
Embracing the Disharmony in Heterogeneous Medical Data

Rongguang Wang^{1,2}, Pratik Chaudhari¹, and Christos Davatzikos^{1,2,3}

¹Department of Electrical and Systems Engineering, University of Pennsylvania

²Center for Biomedical Image Computing and Analytics, University of Pennsylvania

³Department of Radiology, Perelman School of Medicine, University of Pennsylvania
{rgw@seas, pratikac@seas, Christos.Davatzikos@penmedicine}.upenn.edu

Abstract

Heterogeneity in medical imaging data is often tackled, in the context of machine learning, using domain invariance, i.e. deriving models that are robust to domain shifts, which can be both within domain (e.g. demographics) and across domains (e.g. scanner/protocol characteristics). However this approach can be detrimental to performance because it necessitates averaging across intra-class variability and reduces discriminatory power of learned models, in order to achieve better intra- and inter-domain generalization. This paper instead embraces the heterogeneity and treats it as a multi-task learning problem to explicitly adapt trained classifiers to both inter-site and intra-site heterogeneity. We demonstrate that the error of a base classifier on challenging 3D brain magnetic resonance imaging (MRI) datasets can be reduced by 2–3 \times , in certain tasks, by adapting to the specific demographics of the patients, and different acquisition protocols. Learning the characteristics of domain shifts is achieved via auxiliary learning tasks leveraging commonly available data and variables, e.g. demographics. In our experiments, we use gender classification and age regression as auxiliary tasks helping the network weights trained on a source site adapt to data from a target site; we show that this approach improves classification accuracy by 5-30% across different datasets on the main classification tasks, e.g. disease classification.

1 Introduction

Heterogeneity is very common in medical data; Magnetic resonance imaging (MRI) images show dramatic variability across gender, age, race, site at which the data was collected or the specific acquisition protocol used to collect the data [3, 12]. It is challenging to build machine learning-based classifiers for such data, especially if we seek relatively subtle disease effects in the presence of such confounding variability. One may learn invariant representations using domain adaptation techniques [9, 15, 11, 12, 14] but such models are forced to average-out the intraclass variability and sometimes may even decrease single-site performance [3]. An alternative strategy is to stratify the data and tackle each distinct scenario separately but this entails a large variance in the predictions and very large training sets; variants of this approach that employ semi-supervised learning [9], or unsupervised learning [10, 11, 17, 5] often fall short on performance. Further, an often overlooked requirement for domain adaptation methods that is important in practice is that these methods require access to both source and target data, such access is difficult to obtain for medical data due to privacy concerns or scarcity of certain disease-related labels.

This paper embraces the heterogeneity in data. Instead of building models that are invariant to heterogeneity, we design methods that can *adapt* a trained model to specialize on a particular subgroup of the cohort. We focus on classifying Alzheimer’s disease (AD) using atlas-aligned 3D

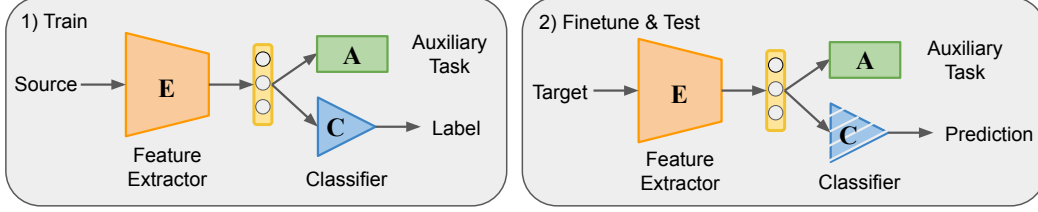


Figure 1: **Overview of multi-site adaptation.** We first jointly train the main task (C), namely classification, and the auxiliary task (A) with a shared feature extractor (E) using labeled images from the source site. Next, we fine-tune the feature extractor on the auxiliary task using samples from the target site. The fine-tuned encoder and the classifier are used at test time to provide predictions. Shaded area indicates that weights of the classifier are fixed.

MRI images of the patients. We demonstrate two specific types of adaptation. First, for *intra-site adaptation* we use data from (readily available) demographic features of the patients (such as age, gender and race) and acquisition protocols to improve performance on these sub-groups. Second, for *inter-site adaptation*, we design auxiliary tasks such as gender classification and age regression that help adapt the main task, namely classifying AD versus controls to a new site; using these auxiliary tasks is convenient because labels for these tasks can be easily obtained on the target site, even at inference time. Further, our adaptation methods do not require having access to data from the source site at inference time.

2 Single-Site Domain Localization

Consider a deep neural network-based classifier with parameters $\theta = (\theta_1, \dots, \theta_K)$ where K denotes the number of layers. Assume we have training data $\mathcal{D} = \{(x_i, y_i)\}_{i=1}^N$ and testing data $\mathcal{D}_t = \{(x_i, y_i)\}_{i=1}^{N_t}$, where $y_i \in C$ for finite set of classes C , from a single-site. We first train the model on all the data, regardless of its heterogeneity, by minimizing the cross-entropy loss $\theta^* = \arg \min_{\theta} \frac{1}{N} \sum_{(x,y) \in \mathcal{D}} -\log p(y | x; \theta)$. We next fine-tune the entire model θ^* on a specific subgroup of the cohort e.g., all the samples within a certain age range, race, or scanner type, $\mathcal{D}^s = \{(x_i^s, y_i^s)\}_{i=1}^M$, where $\mathcal{D}^s \subseteq \mathcal{D}$. This fine-tuning phase solves for

$$\Theta^* = \arg \min_{\Theta} \frac{1}{M} \sum_{(x^s, y^s) \in \mathcal{D}^s} -\log p(y^s | x^s; \Theta) + \frac{\alpha}{2} \|\Theta - \theta^*\|_2^2 + \frac{\beta}{2} \|\Theta\|_2^2. \quad (1)$$

Besides the standard cross-entropy loss, we add the L2-SP regularizer [8] to encourage the final solution Θ^* to be close to the initial model θ^* ; this approach is similar to those in the literature on doubly robust estimation [13] and use weight decay to avoid overfitting.

3 Multi-Site Domain Generalization

Given training data $\mathcal{D}_s = \{(x_i, y_i^c, y_i^a)\}_{i=1}^{N_s}$ from source site and testing data $\mathcal{D}_t = \{(x_i, y_i^a)\}_{i=1}^{N_t}$ from target site, where y_i^c are labels for the main task, y_i^a are labels for the auxiliary task, and each of them are in finite set of categories, we aim to maximize the categorical prediction performance of the classifier on images in the target site on the main task. Similar to the formulation in single-site, we introduce an auxiliary task that shares a portion of the model parameters $\theta_e = (\theta_1, \dots, \theta_{\kappa})$, where $\kappa \in \{1, \dots, K\}$. As Figure 1 shows, we denote the shared parameters θ_e as feature extractor (E) and the unshared parameters $\theta_c = (\theta_{\kappa+1}, \dots, \theta_K)$ as classifier (C). The auxiliary task (A) has its own task-specific parameters $\theta_a = (\theta'_{\kappa+1}, \dots, \theta'_K)$. Since the auxiliary tasks used in this paper are essentially supervised learning, the architecture of the two branches are the same, except for the task-specific output layer dimension. Our proposed multi-site domain generalization approach works in three phases as Figure 1 shows. Firstly, we jointly train the main task, namely, classification, and the auxiliary task in multi-task learning [2] fashion; the model is trained on the same input data $x_i \in \mathcal{D}_s$ for both tasks but with different labels $(y_i^c, y_i^a) \in \mathcal{D}_s$ for each task separately. For auxiliary

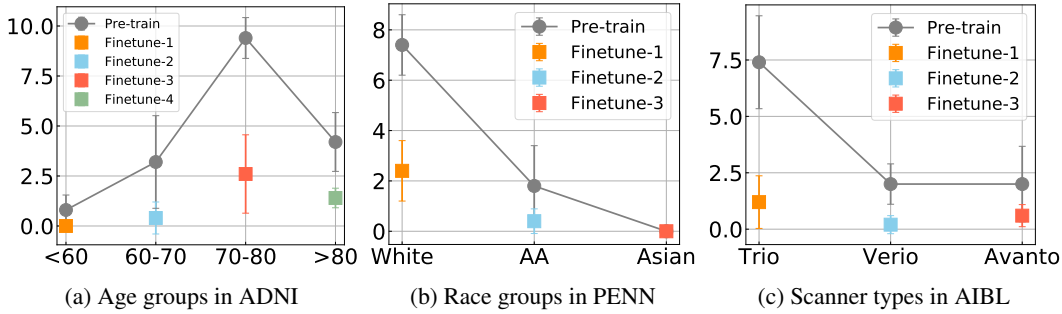


Figure 2: **Test error (in number) on domain-specific groups within each site.** The y-axis is the number of wrong predictions. The grey points show the performance of the pre-trained model, and the colored squares represent the fine-tuned models for each domain-specific group. All results are 5-fold cross-validated and described in mean \pm std format.

Table 1: **Domain generalization with supervised auxiliary tasks cross-site.** Baseline is the model trained with labels. w/out Aux represents training without auxiliary task in contrast to w/ Aux. Fine-tune is the model trained with auxiliary task on test data. Sex classification and age estimation are the two auxiliary tasks. Two loss functions (MSE and Huber) are used for age estimation.

	Study	Baseline	w/out Aux	Sex		Age (MSE)		Age (Huber)	
				w/ Aux	Fine-tune	w/ Aux	Fine-tune	w/ Aux	Fine-tune
Source	ADNI-1	-	0.9054	0.8243	-	0.8108	-	0.8108	-
Target	PENN	0.9043	0.7826	0.7739	0.8348	0.6609	0.8261	0.6522	0.8348
Source	PENN	-	0.9043	0.9043	-	0.9130	-	0.9130	-
Target	ADNI-1	0.9054	0.5811	0.6486	0.6486	0.5811	0.7703	0.7838	0.7973
Target	ADNI-all	0.9006	0.3975	0.4224	0.4286	0.4783	0.6894	0.6584	0.7702

task with loss function l_a , the joint training problem yields

$$\theta_e^*, \theta_c^*, \theta_a^* = \arg \min_{\theta_e, \theta_c, \theta_a} \frac{1}{N_s} \sum_{(x,y) \in \mathcal{D}_s} -\log p(y^c | x; \theta_e, \theta_c) + \lambda l_a(x, y^a; \theta_e, \theta_a), \quad (2)$$

where λ is a balancing parameter. The loss function l_a can be cross-entropy loss for classification task or mean square error (MSE) for regression task. Next, we fine-tune the shared feature extractor θ_e^* by minimizing the auxiliary task loss l_a on target data $(x_i, y_i^a) \in \mathcal{D}_t$. So the fine-tuning phase solve for

$$\Theta_e^*, \Theta_a^* = \arg \min_{\Theta_e, \Theta_a} \frac{1}{N_t} \sum_{(x,y) \in \mathcal{D}_t} l_a(x, y^a; \Theta_e, \Theta_a). \quad (3)$$

Finally, the model makes prediction using the updated parameters $\Theta = (\Theta_e^*, \theta_c^*)$ on the target site $x_i \in \mathcal{D}_t$. The model might benefits from data augmentation in the fine-tuning phase.

4 Experimental Results

We use multiple 3D brain MRI images of Alzheimer’s disease (AD) patients for evaluation. The dataset specification, network architecture, and implementation details are described in Appendix 5.2.

Single-Site. We perform domain localization experiments on ADNI, PENN, and AIBL studies separately. In ADNI study, we localize the model into 4 age groups including: 1) age less than 60; 2) age between 60 to 70; 3) age between 70 to 80; 4) age larger than 80. The grey line in Figure 2 (a) shows the number of wrong predictions for each age group using the baseline (pre-train) model. After fine-tuning on data from each age group, we obtain 4 domain localized model (colorful squares in the figure) with reduced test error. Specifically, the errors dropped from 0.8 to 0 in group 1, from 3.2 to 0.4 in group 2, from 9.4 to 2.6 in group 3, and from 4.2 to 1.4 in group 4. We also show

the classification accuracy on all test samples (not on specific age group) in Appendix 5.1, which reflects that the fine-tuned models are performing well within each domain but compromises in worse generalization ability. Similarly, we decompose data in PENN study into 3 race groups: 1) white people; 2) African American people; 3) Asian people. The test errors declined from 7.4 to 2.4 in white people group, and from 1.8 to 0.4 in African American group using the fine-tuned models. Since there's only 10 Asian samples, we couldn't observe any improvement in the third group. Finally, the images are obtained from three types of Siemens scanner including 1) Trio; 2) Verio; 3) Avanto in AIBL study. We naturally localize the baseline model into each scanner groups and observed error dropping from 7.4 to 1.2 in Trio group, from 2.0 to 0.2 in Verio group, and from 2.0 to 0.6 in Avanto group.

Cross-Site. The experiments are performed between two sites: ADNI and PENN studies; with one site as source site and the other as target site accordingly. AIBL study is not included because the clinical variables of some samples were not available to us at the time of writing. We evaluate the performance using classification accuracy and the quantitative results are shown in Table 1. The performance of models trained on target site are 0.9043 for PENN, 0.9054 for ADNI-1, and 0.9006 for ADNI-all (includes all phases). We compare our method with vanilla models without auxiliary task. A vanilla model trained on ADNI-1 achieves 0.9054 accuracy but its performance dropped to 0.7826 when testing on PENN. Similarly, training and testing on PENN yields 0.9043, dropping to 0.5811 on ADNI-1 and 0.3975 on ADNI-all in the testing phase. Due to population and acquisition shift, the vanilla models cannot generalize across sites.

Two easily-accessible clinical variables: 1) sex; 2) age are used for supervised auxiliary task in the experiments. Model trained on ADNI-1 with sex classification as auxiliary task has lower accuracy but the fine-tuned model increases the accuracy substantially on PENN from 0.7826 to 0.8348. Similarly, models trained on PENN achieve 0.6486 on ADNI-1 and 0.4224 on ADNI-all (further improved by the fine-tuned model to 0.4286). In age estimation auxiliary tasks, MSE and Huber losses are used separately. Models trained with Huber loss perform better than MSE loss in general. Specifically, model trained and tested on PENN achieves 0.9130 accuracy and increased the testing accuracy from 0.5811 to 0.7973 (21.68% increment) on ADNI-1 and from 0.3975 to 0.7702 (37.27% increment) on ADNI-all.

Broader Impact

Intellectual impact. Heterogeneity is the central challenge for effective machine learning for medical data. Broadly speaking, prevalent approaches to tackling this develop representations that are invariant or insensitive to this variability. Our paper demonstrates a dramatically different intellectual approach. We believe that embracing the heterogeneity, i.e., explicitly adapting a trained classifier to a diverse sub-group in the cohort, leads to dramatic performance improvements for both intra-site variations such as age, gender and race, as well as inter-site variations like acquisition protocols at different hospitals.

Enabling accurate predictions for minorities in population groups. Medical datasets demonstrate significant bias from the clinical studies that they are based on. For instance, the ADNI dataset does not have any data about African-American population groups. If machine learning models are oblivious to heterogeneity, they incur a bias while performing inference on such groups. The methods developed in this paper are a first step towards providing more accurate predictions to these sub-groups.

Privacy concerns with data sharing. Existing domain adaptation methods require the source-site data at hand; this is difficult to achieve in practice because of privacy and legislative concerns around data ownership and sharing. The methods developed in this paper are an innovative workaround for this problem, since we only use auxiliary tasks on the target-site to adapt the base model, we do not need to have the source-site data at hand for adaptation.

Acknowledgments

This work was supported by the National Institute on Aging (grant number 1RF1AG054409) and the National Institute of Mental Health (grant number 5R01MH112070).

References

- [1] Avants, B. B., Epstein, C. L., Grossman, M., and Gee, J. C. (2008). Symmetric diffeomorphic image registration with cross-correlation: evaluating automated labeling of elderly and neurodegenerative brain. *Medical image analysis*, 12(1):26–41.
- [2] Caruana, R. (1997). Multitask learning. *Machine learning*, 28(1):41–75.
- [3] Davatzikos, C. (2019). Machine learning in neuroimaging: Progress and challenges. *NeuroImage*, 197:652.
- [4] Fonov, V. S., Evans, A. C., McKinstry, R. C., Almlí, C., and Collins, D. (2009). Unbiased nonlinear average age-appropriate brain templates from birth to adulthood. *NeuroImage*, (47):S102.
- [5] Ganin, Y., Ustinova, E., Ajakan, H., Germain, P., Larochelle, H., Laviolette, F., Marchand, M., and Lempitsky, V. (2016). Domain-adversarial training of neural networks. *The Journal of Machine Learning Research*, 17(1):2096–2030.
- [6] He, T., Zhang, Z., Zhang, H., Zhang, Z., Xie, J., and Li, M. (2019). Bag of tricks for image classification with convolutional neural networks. In *Proceedings of the IEEE Conference on Computer Vision and Pattern Recognition*, pages 558–567.
- [7] Kingma, D. P. and Ba, J. (2014). Adam: A method for stochastic optimization. *arXiv preprint arXiv:1412.6980*.
- [8] Li, X., Grandvalet, Y., and Davoine, F. (2018). Explicit inductive bias for transfer learning with convolutional networks. *arXiv preprint arXiv:1802.01483*.
- [9] Meng, Q., Rueckert, D., and Kainz, B. (2020). Learning cross-domain generalizable features by representation disentanglement. *arXiv preprint arXiv:2003.00321*.
- [10] Moyer, D., Gao, S., Brekelmans, R., Galstyan, A., and Ver Steeg, G. (2018). Invariant representations without adversarial training. In *Advances in Neural Information Processing Systems*, pages 9084–9093.
- [11] Moyer, D., Ver Steeg, G., Tax, C. M., and Thompson, P. M. (2020). Scanner invariant representations for diffusion mri harmonization. *Magnetic Resonance in Medicine*.
- [12] Pomponio, R., Erus, G., Habes, M., Doshi, J., Srinivasan, D., Mamourian, E., Bashyam, V., Nasrallah, I. M., Satterthwaite, T. D., Fan, Y., et al. (2020). Harmonization of large mri datasets for the analysis of brain imaging patterns throughout the lifespan. *NeuroImage*, 208:116450.
- [13] Reddi, S. J., Póczos, B., and Smola, A. (2015). Doubly robust covariate shift correction. In *Twenty-Ninth AAAI Conference on Artificial Intelligence*. Citeseer.
- [14] Robey, A., Hassani, H., and Pappas, G. J. (2020). Model-based robust deep learning. *arXiv preprint arXiv:2005.10247*.
- [15] Robinson, R., Dou, Q., Castro, D., Kamnitsas, K., de Groot, M., Summers, R., Rueckert, D., and Glocker, B. (2020). Image-level harmonization of multi-site data using image-and-spatial transformer networks. *arXiv preprint arXiv:2006.16741*.
- [16] Tustison, N. J., Avants, B. B., Cook, P. A., Zheng, Y., Egan, A., Yushkevich, P. A., and Gee, J. C. (2010). N4itk: improved n3 bias correction. *IEEE transactions on medical imaging*, 29(6):1310–1320.
- [17] Tzeng, E., Hoffman, J., Saenko, K., and Darrell, T. (2017). Adversarial discriminative domain adaptation. In *Proceedings of the IEEE conference on computer vision and pattern recognition*, pages 7167–7176.
- [18] Wen, J., Thibeau-Sutre, E., Diaz-Melo, M., Samper-González, J., Routier, A., Bottani, S., Dormont, D., Durrleman, S., Burgos, N., Colliot, O., et al. (2020). Convolutional neural networks for classification of alzheimer’s disease: Overview and reproducible evaluation. *Medical Image Analysis*, page 101694.

5 Appendix

5.1 Domain Localization

Table 2: **Domain localization performance in age, race, and scanner groups.** Error # and Total Acc are number of wrong predictions in each group and accuracy on all test data (not on specific group) from 5-fold cross-validation in [mean \pm std] format. Since there’s only one pre-trained model for each study, the Total Acc are the same for each group.

ADNI	Age Group							
	< 60		60 – 70		70 – 80		> 80	
	Error #	Total Acc	Error #	Total Acc	Error #	Total Acc	Error #	Total Acc
Pre-train	0.8 \pm 0.75	0.8904 \pm 0.01	3.2 \pm 2.32	0.8904 \pm 0.01	9.4 \pm 1.02	0.8904 \pm 0.01	4.2 \pm 1.47	0.8904 \pm 0.01
Fine-tune	0.0 \pm 0.00	0.8556 \pm 0.05	0.4 \pm 0.80	0.9141 \pm 0.01	2.6 \pm 1.96	0.9364 \pm 0.02	1.4 \pm 0.49	0.9153 \pm 0.02

PENN	Race Group					
	White		African American		Asian	
	Error #	Total Acc	Error #	Total Acc	Error #	Total Acc
Pre-train	7.4 \pm 1.20	0.9160 \pm 0.01	1.80 \pm 1.60	0.9160 \pm 0.01	0.00 \pm 0.00	0.9160 \pm 0.01
Fine-tune	2.4 \pm 1.20	0.9667 \pm 0.02	0.40 \pm 0.49	0.9213 \pm 0.02	0.00 \pm 0.00	0.9020 \pm 0.02

AIBL	Scanner Type					
	Trio		Verio		Avanto	
	Error #	Total Acc	Error #	Total Acc	Error #	Total Acc
Pre-train	7.4 \pm 2.06	0.8962 \pm 0.01	2.0 \pm 0.89	0.8962 \pm 0.01	2.0 \pm 1.67	0.8962 \pm 0.01
Fine-tune	1.2 \pm 1.17	0.9631 \pm 0.02	0.2 \pm 0.40	0.9102 \pm 0.01	0.6 \pm 0.49	0.9208 \pm 0.02

5.2 Dataset and Implementation

Table 3: **Summary of participant demographics cross studies.** Age is described in format: mean \pm std [min, max]. F and M in gender represent female and male separately. W, B and A in race represent white, black or African American, and Asian separately. Other races or more than one race does not show here. The heterogeneous variables are missing for some subjects in AIBL study.

Study	Subjects	CN	AD	Age	Gender	Race
ADNI-1	369	178	191	75.5 \pm 6.5 [55.0, 90.9]	178 F / 191 M	341 W / 21 B / 5 A
ADNI-2/GO	407	261	146	73.1 \pm 6.8 [55.4, 90.3]	206 F / 201 M	369 W / 21 B / 9 A
ADNI-3	27	24	3	71.0 \pm 7.1 [55.8, 89.2]	18 F / 9 M	27 W / 0 B / 0 A
PENN	572	229	343	72.0 \pm 11.9 [22.6, 95.2]	361 F / 211 M	432 W / 116 B / 10 A
AIBL	568	481	87	-	-	-

Datasets. We use 3D T1-weighted brain magnetic resonance imaging (MRI) scans from three sites, including Alzheimer’s Disease Neuroimaging Initiative¹ (ADNI) study, Penn Medicine (PENN) study, and the Australian Imaging, Biomarkers and Lifestyle² (AIBL) study. Two diagnosis groups are considered in the experiments: 1) cognitive normal (CN): sessions of subjects who were diagnosed as CN at baseline and stayed stable during the follow-up; 2) Alzheimer’s disease (AD): sessions of subjects who were diagnosed as AD at baseline and stayed stable during the follow-up. For pre-processing, all images are bias-field corrected with N4ITK [16] and affinely aligned to MNI [4] space using ANTs [1]. The final image size is 193 \times 229 \times 193 with 1 mm³ isotropic voxels. Before feeding into the network, the intensity of images are normalised to zero mean and unit variance.

Network details. We use 3D subject-level neural network for better performance and we design the architecture based on [18]. The feature extractor (E) is stacked by 5 convolutional blocks, where each block consists of convolution layer, batch normalization, ReLU nonlinearity, and max pooling. We increased the kernel size of convolution operation to 5, which improved the reception filed. We use a three-layer multilayer perceptron (MLP) with ReLU nonlinearity for the classifier (C) and same for

¹<http://adni.loni.usc.edu>

²<https://aibl.csiro.au>

the auxiliary task (A). This light-weight model shows comparable performance to "standard" ResNet or Wide ResNet in our experiment, and we benefit in memory and computational efficiency.

Implementation details. Our architectures and hyper-parameters are consistent across all experiments. We use Adam [7] with initial learning rate $1e - 4$ and weight decay $1e - 5$ for training. A learning rate scheduler with cyclic cosine annealing [6] is used for better convergence. We use batch size of 6 and the training phase stops in at most 60 epochs. The training naturally benefits from data augmentation techniques. We randomly apply Gaussian blur filter on the input data in online fashion. For fine-tuning in single-site domain localization experiment, we choose $\alpha = 0.1$ and $\beta = 0.01$ as suggested in [8]. For joint training in cross-site domain generalization experiment, we choose $\lambda = 1$ for auxiliary task using cross-entropy as loss function, and $\lambda = 0.1$ for those who use mean square error (MSE) or Huber loss.